

Non-frequency-selective I/Q Imbalance in Zero-IF Transceivers for Wide-Band mmW Links

Ainhoa Rezola, Juan Francisco Sevillano,
Roc Berenguer, Igone Vélez

Centro de Estudios e Investigaciones Técnicas (CEIT)
San Sebastián, Spain
Email: {argarciandia,jfsevillano,
rberenguer,ivelez}@ceit.es

Martin Leyh, Moises Lorenzo,
Aharon Vargas

Fraunhofer Institute for Integrated Circuits (IIS)
Erlangen, Germany
Email: {martin.leyh,moises.lorenzo,
aharon.vargas}@iis.fraunhofer.de

Abstract—Millimeter wave (mmW) links are an attractive solution for backhaul of mobile networks. In order to cope with the requirements of future networks, these mmW links should achieve Gigabit data rates. These data rates can be achieved using wide-band and high order modulations in E-Band. Zero-IF architectures are good candidates for integrated transceivers. However, the design of integrated transceivers at these frequencies is a challenging issue. An important source of degradation is I/Q imbalance, which can significantly reduce the performance of a communication system with zero-IF transceivers if it is not appropriately compensated. In this paper, the impact of the I/Q imbalance impairment on the transmitted and received signal is analyzed and suitable digital signal processing techniques are evaluated for I/Q imbalance compensation at the receiver for a 64-QAM system using 2GHz bandwidth.

Keywords—Mobile backhaul; millimeter-wave; transceivers; RF impairments.

I. INTRODUCTION

The growing demand for ubiquitous broadband communication, e.g., fourth-generation (4G) wireless, has motivated the deployment of ultra high-speed communication systems. Especially in backhauling networks, optical fiber is required to transport very high data rates. However, optical fiber exhibits important drawbacks, such as high costs, long deployment times, and low flexibility. Recently, point-to-point wireless communication systems have been proposed as an attractive alternative to optical fiber. In order to achieve comparable data rates as the optical fiber, these communication systems demand a very high bandwidth to transport enough data. Although the frequency spectrum is congested, the regulation of the E-band facilitates the deployment of high-speed communication systems. The European Telecommunications Standards Institute (ETSI) is carrying out a standardization process for this frequency band [1][2].

Commercial off-the-shelf communication systems operating in the E-band support data rates up to 2.5 Gbit/s. However, new applications demand even higher data rates, which necessitate both wide-band and high-order modulations to utilize the spectrum efficiently. Higher order modulations require high Carrier-to-Interference (C/I) ratios at the receiver involving careful analysis of the degradation effects introduced by the analog Radio-Frequency (RF) impairments and evaluation of corresponding compensation algorithms in the digital baseband processing [3].

In this paper, we focus on the I/Q imbalance impairment caused by the local oscillators used for quadrature modulation and demodulation in zero-IF transceivers. In an ideal quadrature modulator or demodulator, the mirror images are completely suppressed. I/Q imbalance entails a degradation in the Image Rejection Ratio (IRR) and causes interfering images at mirror frequencies [4]. The paper analyzes the impact of these local oscillator imbalances in the transmitted and received signal. Building upon the results of this analysis, an approach to compensate for both transmitter and receiver induced I/Q imbalance by digital signal processing techniques is selected and its performance for a 64-QAM transceiver operating with a signal bandwidth of 2GHz is evaluated.

Section II introduces the I/Q imbalance issue identifying and modeling the source of this impairment. The mitigation of the I/Q imbalance impairment by digital signal processing at the receiver is described in Section III. In Section IV, the selected mechanism to cope with the I/Q imbalance is simulated and analyzed. Finally, some conclusions are drawn in Section V.

II. SYSTEM ANALYSIS

A. Transceiver architecture

In order to address new applications for the future backhauling networks, a point-to-point microwave link in the E-Band using a 64-QAM modulation with a signal bandwidth of 2GHz is considered. Figure 1 shows the proposed transceiver (TRx) architecture for a point-to-point microwave link in the E-Band. As shown, the transmitter (Tx) front-end consists of an I/Q up-converting modulator that up-converts the baseband I and Q channels to an Intermediate Frequency (IF). After combining the I and Q channels, the IF signal is up-converted by means of the millimeter-wave (mmW) mixer. The receiver (Rx) front-end consists of a wideband Low Noise Amplifier (LNA), which receives and amplifies the signal at the E-Band. After the LNA, a first mixer down-converts the mmW signal to the same IF as in the Tx. This way, the same PLL can be re-used for the Tx and the Rx. Finally, an I/Q demodulator down-converts the IF signal to 0-Hz.

This architecture presents a good balance between different design aspects and enables to minimize the sampling frequency of the Digital-to-Analog (DAC) and Analog-to-Digital (ADC) Converters. Nowadays, we can find commercial DACs and

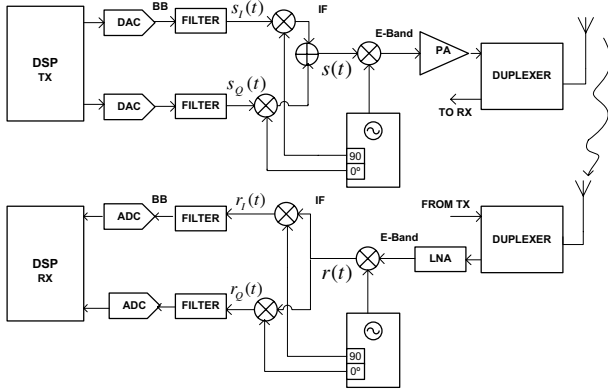


Figure 1. Architecture of the transceiver.

ADCs able to provide sampling rates close to 3Gps, which is enough for practical implementation of the zero-IF architecture. The use of other architectures such as low-IF would require very high performance DACs or ADCs, with sampling rates well above 4Gps to achieve a practical implementation of base-band and image rejection filters in the analog front-end.

However, this zero-IF architecture is subject to the corruption due to I/Q imbalances at the transmitter and receiver quadrature modulator and demodulator respectively. The resulting system performance degradation can be important, specially for high-order modulation schemes [5].

B. I/Q Imbalance Analysis

The goal of the I/Q modulator in Figure 1 is to perform a frequency translation of the signal. That is, if the base-band input signal to the I/Q modulator is

$$\tilde{s}(t) = s_I(t) + js_Q(t), \quad (1)$$

where $s_I(t)$ is the signal in the I-datapath and $s_Q(t)$ is the signal in the Q-datapath, a perfect I/Q modulation mixes the base-band input signal with

$$l_{tx}(t) = e^{j\omega_{tx}t} = \cos(\omega_{tx}t) + j \sin(\omega_{tx}t) \quad (2)$$

producing an output signal

$$s(t) = \text{Re}[\tilde{s}(t)l_{tx}(t)] = s_I(t) \cos(\omega_{tx}t) - s_Q(t) \sin(\omega_{tx}t). \quad (3)$$

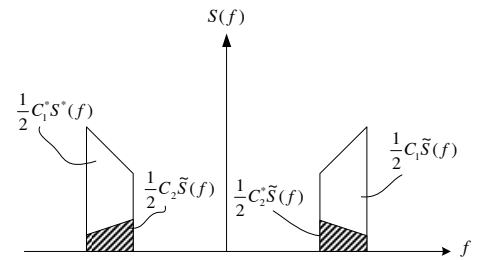
However, when implementing an I/Q modulator with actual electronic circuits, the signals produced by the Local Oscillator (LO) will present some difference in their amplitudes and will not have a phase difference of $\pi/2$. The effect of this imbalance can be modeled as the mixing of the base-band input signal with

$$l_{tx}(t) = \cos(\omega_{tx}t) + jg_{tx} \sin(\omega_{tx}t + \phi_{tx}) \quad (4)$$

to yield the output signal

$$s(t) = (s_I(t) - g_{tx} \sin(\phi_{tx})s_Q(t)) \cos(\omega_{tx}t) \quad (5a)$$

$$- s_Q(t)g_{tx} \cos(\phi_{tx}) \sin(\omega_{tx}t). \quad (5b)$$


 Figure 2. Spectrum of $s(t)$ with imbalance.

In I/Q imbalance analysis, it is common to rewrite the signal produced at the transmitter LO with imbalance of (4) in the form [6]

$$l_{tx}(t) = C_1 e^{j\omega_{tx}t} + C_2 e^{-j\omega_{tx}t}, \quad (6)$$

with

$$C_1 = \frac{1 + g_{tx} e^{j\phi_{tx}}}{2} \quad (7a)$$

$$C_2 = \frac{1 - g_{tx} e^{-j\phi_{tx}}}{2} \quad (7b)$$

and the transmitted signal is

$$s(t) = \text{Re}[\tilde{s}(t) (C_1 e^{j\omega_{tx}t} + C_2 e^{-j\omega_{tx}t})]. \quad (8)$$

In (8), the desired term is the one multiplied by $e^{j\omega_{tx}t}$ and the term multiplied by $e^{-j\omega_{tx}t}$ is considered an undesired image. Working on (8) we can rewrite it as

$$s(t) = \frac{1}{2} (C_1 \tilde{s}(t) e^{j\omega_{tx}t} + C_1^* \tilde{s}^*(t) e^{-j\omega_{tx}t}) \quad (9a)$$

$$+ \frac{1}{2} (C_2^* \tilde{s}^*(t) e^{j\omega_{tx}t} + C_2 \tilde{s}(t) e^{-j\omega_{tx}t}), \quad (9b)$$

where $(\cdot)^*$ denotes the complex conjugate.

Let $X(\omega)$ denote the Fourier Transform of a signal $x(t)$, then from (9) we have

$$S(\omega) = \frac{1}{2} (C_1 \tilde{S}(\omega - \omega_{tx}) + C_1^* \tilde{S}^*(\omega + \omega_{tx}) \quad (10a)$$

$$+ C_2^* \tilde{S}^*(\omega - \omega_{tx}) + C_2 \tilde{S}(\omega + \omega_{tx})) \quad (10b)$$

Figure 2 illustrates the spectrum of $s(t)$. The first line in the above equation is the desired term and the second line is an image that aliases on the desired signal. A measure of performance of the I/Q modulator is the Image Rejection Ratio (IRR)

$$\text{IRR}_{tx} = \frac{|C_1|^2}{|C_2|^2} = \frac{1 + g_{tx}^2 + 2g_{tx} \cos(\phi_{tx})}{1 + g_{tx}^2 - 2g_{tx} \cos(\phi_{tx})}. \quad (11)$$

Similarly, the task of the Rx I/Q demodulator in Figure 1 is to mix the input signal with

$$l_{rx}(t) = e^{-j\omega_{rx}t} = \cos(\omega_{rx}t) - j \sin(\omega_{rx}t), \quad (12)$$

so that after low-pass filtering, we get the base-band equivalent of the signal in the frequency band of interest $\tilde{z}(t) = z_I(t) + jz_Q(t)$. Note that $\tilde{z}(t)$ is the base-band equivalent referred to a carrier frequency ω_{rx} . The actual implementation of the I/Q

demodulator will introduce similar imbalances to the actual implementation of the I/Q modulator, which can be modeled as the mixing of $r(t)$ with

$$l_{rx}(t) = \cos(\omega_{rx}t) - jg_{rx} \sin(\omega_{rx}t + \phi_{rx}). \quad (13)$$

The signal at the output of the I/Q demodulator after low-pass filtering can be written as [6]

$$\tilde{r}(t) = r_I(t) + jr_Q(t) = K_1\tilde{z}(t) + K_2\tilde{z}^*(t) \quad (14)$$

with

$$K_1 = \frac{1 + g_{rx}e^{-j\phi_{rx}}}{2} \quad (15a)$$

$$K_2 = \frac{1 - g_{rx}e^{j\phi_{rx}}}{2}. \quad (15b)$$

In this case, the first term in the sum of (14) is the desired term and the second one is the image that aliases on the desired signal. The IRR for the I/Q demodulator is defined as

$$\text{IRR}_{rx} = \frac{|K_1|^2}{|K_2|^2} = \frac{1 + g_{rx}^2 + 2g_{rx} \cos(\phi_{rx})}{1 + g_{rx}^2 - 2g_{rx} \cos(\phi_{rx})}. \quad (16)$$

Note that the above model for the impairment affects in the same way to the whole information bearing signal. Thus, the I/Q imbalance is said to be Non-Frequency-Selective (NFS). Other imbalances in the in-phase and quadrature datapaths of the information bearing signals can introduce Frequency-Selective (FS) I/Q imbalance. In this paper, we restrict our attention to the NFS component of the I/Q imbalance. Although the model has been developed from the point of view of the local oscillators of the I/Q modulator and demodulator, it can also be used to include the mean imbalances between the in-phase and quadrature datapaths.

In order to gain some insight, we assume enough linearity and proper filtering in the remaining stages of the transmitter and receiver analog chain and noise-less operation. Using (9), it can be seen that

$$\tilde{z}(t) = (C_1\tilde{s}(t) + C_2^*\tilde{s}^*(t))e^{j(\Delta\omega t + \theta)} \quad (17)$$

where $\Delta\omega$ and θ account for the overall carrier frequency and phase offset between the transmitter and the receiver. Thus, we have

$$\tilde{r}(t) = K_1C_1\tilde{s}(t)e^{j(\Delta\omega t + \theta)} \quad (18a)$$

$$+ K_1C_2^*\tilde{s}^*(t)e^{j(\Delta\omega t + \theta)} \quad (18b)$$

$$+ K_2C_1^*\tilde{s}^*(t)e^{-j(\Delta\omega t + \theta)} \quad (18c)$$

$$+ K_2C_2\tilde{s}(t)e^{-j(\Delta\omega t + \theta)} \quad (18d)$$

The desired term in (18) is the one in the first line and the terms in the second to fourth line represent undesired images at the receiver due to transmitter and receiver I/Q imbalances.

When $\Delta\omega = 0$, (18) simplifies to

$$\tilde{r}(t) = J_1\tilde{s}(t) + J_2\tilde{s}^*(t) \quad (19)$$

where J_1 and J_2 are constants given by

$$J_1 = K_1C_1e^{j\theta} + K_2C_2e^{-j\theta} \quad (20a)$$

$$J_2 = K_1C_2^*e^{j\theta} + K_2C_1^*e^{-j\theta}. \quad (20b)$$

Comparing (19) with (14), it can be concluded that when $\Delta\omega = 0$, the effect observed at the output of the receiver's

I/Q demodulator due to the I/Q imbalance introduced at the transmitter is the same as the one due to an I/Q imbalance introduced by the I/Q demodulator. In a real transmission system there will be some carrier frequency offset between the transmitter and the receiver. However, the former observation suggests that the I/Q imbalance introduced at the transmitter may be addressed after carrier frequency recovery using approaches designed to address the I/Q imbalance introduced at the receiver.

III. I/Q IMBALANCE COMPENSATION

A. Tx I/Q Imbalance Compensation

Using (1) and (3) with $\tilde{s}'(t) = s'_I(t) + js'_Q(t)$ denoting the equivalent baseband signal of the Tx I/Q distorted signal $s(t)$ with respect to the transmitter carrier frequency ω_{tx} , we can derive the following matrix equation for Tx I/Q imbalance distortion:

$$\begin{bmatrix} s'_I(t) \\ s'_Q(t) \end{bmatrix} = \begin{bmatrix} 1 & -g_{tx} \sin(\phi_{tx}) \\ 0 & g_{tx} \cos(\phi_{tx}) \end{bmatrix} \begin{bmatrix} s_I(t) \\ s_Q(t) \end{bmatrix}. \quad (21)$$

If the matrix in (21) is invertible ($g_{tx} \neq 0$ and $\phi_{tx} \neq \pm\pi/2$), what is the case for practical cases, the Tx NFS I/Q compensation can ideally be achieved by performing a digital predistortion based on the inverse operation. In this case, we feed the I/Q modulator with the predistorted signal $\zeta(t) = \zeta_I(t) + j\zeta_Q(t)$, which is obtained as

$$\begin{bmatrix} \zeta_I(t) \\ \zeta_Q(t) \end{bmatrix} = \begin{bmatrix} 1 & \tan(\phi_{tx}) \\ 0 & 1/(g_{tx} \cos(\phi_{tx})) \end{bmatrix} \begin{bmatrix} s_I(t) \\ s_Q(t) \end{bmatrix}, \quad (22)$$

Compensation by inverse transformation requires knowledge of the gain and phase imbalance values, g_{tx} and ϕ_{tx} .

Techniques for compensation of the transmitter I/Q imbalance at the transmitter have been proposed in the literature using tones as test signals (e.g., [7][8][9][10]) or even from random data (e.g., [8][11]). The compensation using test tones is very powerful and can be used for initial calibration. During normal full-duplex operation of the transceiver, I/Q imbalance compensation from the random transmitted data would be preferred. All these techniques of compensation require additional circuitry (including an extra ADC) at the transmitter to feedback measurements performed in the analog front-end.

Under certain conditions Tx I/Q imbalance can also be compensated in the receiver [6]. For this to be possible, an important issue is that the spectral images caused by Tx I/Q imbalance have to be emitted. This condition is fulfilled in the analyzed system. Receiver-based compensation of Tx I/Q imbalance is the approach further investigated in this paper, because it does not require any additional circuitry in the analog front-end of the transceiver and all the compensation can be performed by digital signal processing.

B. Rx I/Q Imbalance Compensation

The down-converted complex-valued base-band signal $\tilde{r}(t)$ can be written as a function of $\tilde{z}(t)$ using the following matrix equation

$$\begin{bmatrix} r_I(t) \\ r_Q(t) \end{bmatrix} = \begin{bmatrix} 1 & 0 \\ -g_{rx} \sin(\phi_{rx}) & g_{rx} \cos(\phi_{rx}) \end{bmatrix} \begin{bmatrix} z_I(t) \\ z_Q(t) \end{bmatrix}. \quad (23)$$

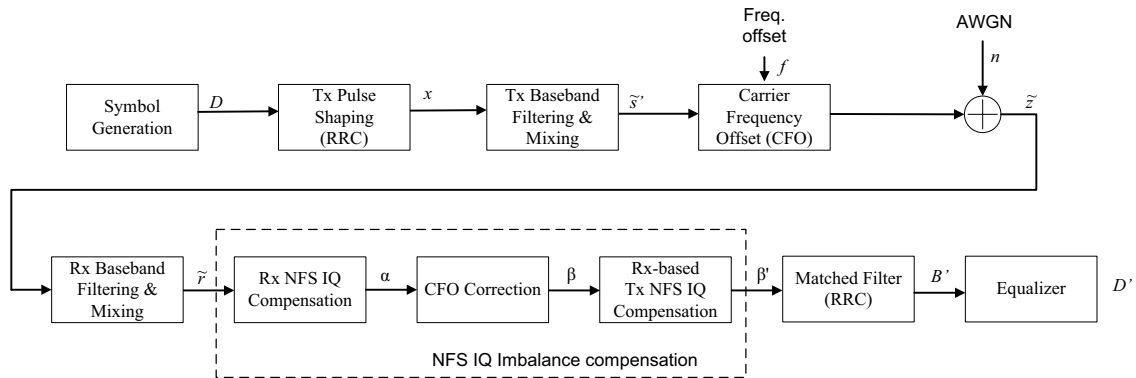


Figure 3. System Model for I/Q Imbalance Simulations.

In case the matrix in (23) is invertible ($g_{rx} \neq 0$ and $\phi_{rx} \neq \pm\pi/2$), what is the case for practical cases, the Rx I/Q imbalance can be ideally compensated by performing the inverse operation

$$\begin{bmatrix} \alpha_I(t) \\ \alpha_Q(t) \end{bmatrix} = \begin{bmatrix} 1 & 0 \\ \tan(\phi_{rx}) & 1/(g_{rx} \cos(\phi_{rx})) \end{bmatrix} \begin{bmatrix} z'_I(t) \\ z'_Q(t) \end{bmatrix}, \quad (24)$$

where $\alpha(t) = \alpha_I(t) + j\alpha_Q(t)$ is the output of the Rx I/Q imbalance compensator and ideally would yield the desired baseband signal $\tilde{z}(t)$. Compensation by inverse transformation requires knowledge of the gain and phase imbalance values g_{rx} and ϕ_{rx} , which can be derived by using statistics and correlation properties of the I and Q signals as proposed in [12].

IV. SIMULATION RESULTS

A. System Model

Figure 3 depicts the simulation model developed in Matlab for the analysis of the I/Q imbalance in the transceiver performance. Random data information is generated as a sequence of I/Q symbols, D , by using a 64-QAM mapper. D is then filtered through an appropriate Root-Raised-Cosine (RRC) filter to create a pulse-shaped base-band signal x . The Tx Baseband Filtering and Mixing models the data processing in the transmitter analog front-end shown in Figure 1, including the NFS-I/Q imbalance at the I/Q modulator.

Considering an Additive White Gaussian Noise (AWGN) channel, the signal \tilde{z} at the output of the channel model is given by:

$$\tilde{z}(t) = \tilde{s}'(t) \cdot e^{j2\pi ft} + n(t), \quad (25)$$

where $\tilde{z}(t)$ is the low-pass equivalent of the transmitted signal, with f the Carrier Frequency Offset (CFO) in Hz. Finally, $n(t)$ corresponds to a complex-valued white Gaussian noise process.

On the receiver side, the Rx Baseband Filtering and Mixing models the receiver analog front-end structure shown in Figure 1 including Rx I/Q imbalance. NFS I/Q Imbalance Compensation is performed prior to matched filtering following a multi-stage approach that compensates for both Tx and Rx I/Q Imbalance:

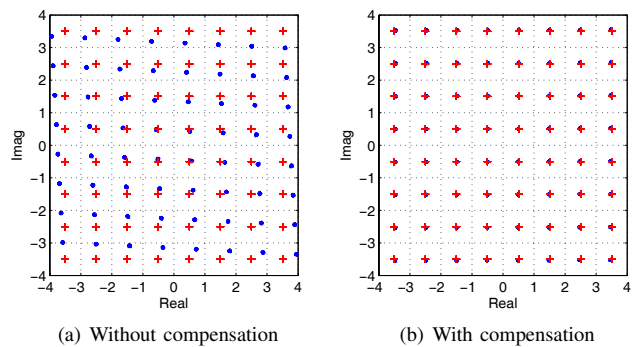


Figure 4. NFS I/Q imbalance

- 1) The first stage compensates for the Rx NFS I/Q imbalance based on the algorithms in Section III.
- 2) A CFO correction stage compensates for the CFO.
- 3) A third stage is employed for performing Tx NFS I/Q imbalance compensation prior to the matched filter by applying again the algorithms in Section III.

The NFS I/Q compensated signal, β' , is then filtered with a matched RRC filter in order to recover the transmitted information. Due to the high bandwidth of the signal and limited sampling rates of the DACs and ADCs, there is a frequency selectivity in the analog chain of the system. So as to compensate for this frequency response, an equalizer modelled as a Wiener filter [13] has been included at the receiver. The received symbols D' are then compared with the transmitted symbols D to quantify the performance of the whole system.

B. Results

Figure 4(a) illustrates the effect of NFS I/Q imbalance. For illustration purpose, a noiseless transmission is considered. Crosses correspond to the constellation when perfect transmission takes place, and the dots correspond to a transmission with I/Q imbalances both at transmitter and receiver assuming zero carrier frequency offset. The I/Q imbalances considered were 0.5 dB and 3 degrees in gain and phase, respectively, in the transmitter and 1 dB and 3 degrees in gain and phase, respectively, in the receiver. The signs of the imbalances

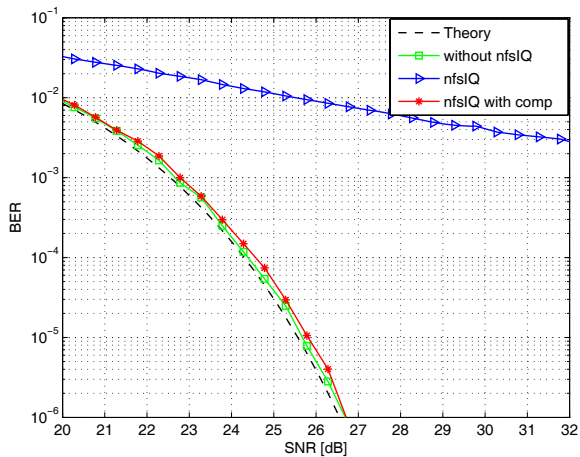
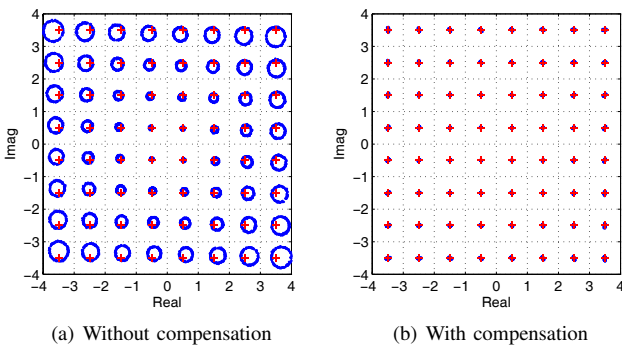


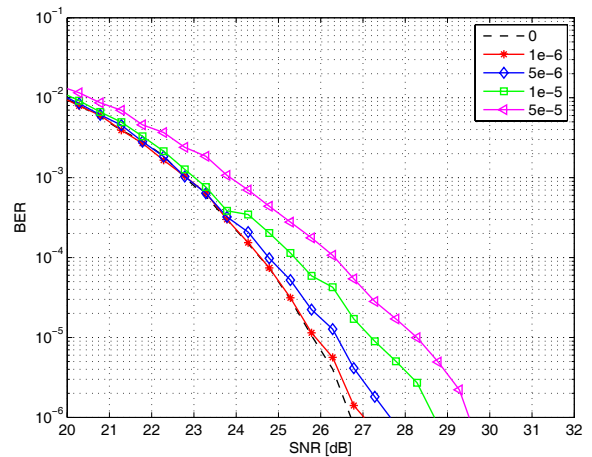
Figure 5. System performance in the presence of NFS I/Q imbalance.


 Figure 6. NFS I/Q imbalance with normalized residual carrier frequency offset $\Delta\omega T/(2\pi) = 5 \cdot 10^{-6}$.

were selected in the transmitter and the receiver so that they combine in the worst possible distortion. Figure 4(b) shows the constellation at the receiver when the NFS I/Q imbalance compensation is active. As it can be seen, the NFS I/Q imbalance compensation approach is able to remove the distortion of the constellation.

Figure 5 shows the impact of the NFS I/Q imbalance in the performance of the transceiver. The curve labeled ‘without NFS IQ’ is the performance of the transceiver when there is no I/Q imbalance. As it is shown in the figure the equalizer used to compensate the frequency selectivity of the analog chain introduces minor losses. The curve labeled ‘NFS IQ’ is the performance of the transceiver with I/Q imbalance at both transmitter and receiver. The curve labeled ‘NFS IQ with comp’ is the performance when the I/Q imbalance compensation is active. The NFS I/Q imbalance compensation is able to reduce the losses to a few tenths of a dB.

Figure 6(a) illustrates the effect of NFS I/Q imbalance when there is a residual carrier frequency offset equal to $\Delta\omega = 2\pi \cdot 5 \cdot 10^{-6}/T$ after the CFO correction in Figure 3, with T the symbol period. For proper symbol detection and BER estimation, the residual carrier frequency offset has been compensated in the simulations at the input of the receiver’s matched-filter. The figure shows the corrected constellations


 Figure 7. Performance of NFS I/Q imbalance compensation approach for different values of $\Delta\omega T/(2\pi)$.

after this final residual carrier frequency offset compensation. The transmitter’s I/Q imbalance manifests itself as rotations of the constellation around the distorted constellation due to the receiver’s I/Q imbalance.

Figure 6(b) shows the constellation when the I/Q compensation algorithms are active for the same residual carrier frequency offset. It can be seen that a reduction in the distortion of the constellation has been achieved despite some residual carrier frequency offset.

Figure 7 shows the impact of residual carrier frequency offset on the performance of the NFS I/Q imbalance compensation approach presented in Section III. The different curves correspond to different values of the normalized residual carrier frequency offset $\Delta\omega T/(2\pi)$. It can be seen that a very accurate carrier frequency offset correction is needed for proper compensation of the transmitter I/Q imbalance with residual CFO below $\Delta\omega T/(2\pi) = 5 \cdot 10^{-6}$, what can be achieved via application of state of the art coarse and fine frequency synchronization algorithms [14].

V. CONCLUSION

In this paper, a theoretical analysis of the NFS I/Q imbalance in a zero-IF transceiver has been presented. Digital signal processing at the receiver has been evaluated based on a multi-stage approach for the compensation of both transmitter and receiver I/Q imbalance, as well as carrier frequency offset.

Simulation results were presented for a zero-IF transceiver using 64-QAM with a signal bandwidth of 2GHz. The simulation results show that receiver-based Tx I/Q imbalance compensation can be achieved with negligible degradation in overall system performance. This is achieved when accurate frequency synchronization is performed in the receiver that reduces the residual carrier frequency offset below specified limits.

ACKNOWLEDGMENT

The research leading to these results has received funding from the European Community’s Framework Programme

FP7/2007-2013 under grant agreement no. 317957. Consortium: Ceit, FhG, ALU-I, CEA-Leti, INCIDE, SiR, ST-I, Silvers IMA, OTE.

REFERENCES

- [1] Fixed Radio Systems; Characteristics and requirements for point-to-point equipment and antennas; Part 1: Overview and system-independent common characteristics, ETSI EN 302 217-1, Sept. 2012.
- [2] Fixed Radio Systems; Characteristics and requirements for point-to-point equipment and antennas; Part 2-2: Digital systems operating in frequency bands where frequency co-ordination is applied; Harmonized EN covering the essential requirements of article 3.2 of the R&TTE Directive, ETSI EN 302 217-2-2, Sept. 2012.
- [3] G. Fettweis et al., "Dirty RF: a new paradigm," in Personal, Indoor and Mobile Radio Communications, 2005. PIMRC 2005. IEEE 16th International Symposium on, vol. 4, 2005, pp. 2347–2355 Vol. 4.
- [4] M. Valkama, M. Renfors, and V. Koivunen, "Advanced methods for I/Q imbalance compensation in communication receivers," IEEE Transactions on Signal Processing, vol. 49, no. 10, 2001, pp. 2335–2344.
- [5] B. Razavi, "Design considerations for direct-conversion receivers," Circuits and Systems II: Analog and Digital Signal Processing, IEEE Transactions on, vol. 44, no. 6, 1997, pp. 428–435.
- [6] L. Antilla, "Digital Front-End Processing with Widely-Linear Signal Models in Radio Devices," Ph.D. dissertation, Tampere University of Technology, 2011.
- [7] J. Cavers and M. Liao, "Adaptive compensation for imbalance and offset losses in direct conversion transceivers," Vehicular Technology, IEEE Transactions on, vol. 42, no. 4, 1993, pp. 581–588.
- [8] J. Cavers, "New methods for adaptation of quadrature modulators and demodulators in amplifier linearization circuits," Vehicular Technology, IEEE Transactions on, vol. 46, no. 3, 1997, pp. 707–716.
- [9] A. Nassery, S. Byregowda, S. Ozev, M. Verhelst, and M. Slamani, "Built-in-self test of transmitter i/q mismatch using self-mixing envelope detector," in VLSI Test Symposium (VTS), 2012 IEEE 30th, 2012, pp. 56–61.
- [10] S. D'Souza et al., "A 10-bit 2-gs/s dac-ddfs-iq-controller baseband enabling a self-healing 60-ghz radio-on-chip," Circuits and Systems II: Express Briefs, IEEE Transactions on, vol. 60, no. 8, 2013, pp. 457–461.
- [11] X. Huang and M. Caron, "Efficient transmitter self-calibration and amplifier linearization techniques," in Circuits and Systems, 2007. ISCAS 2007. IEEE International Symposium on, 2007, pp. 265–268.
- [12] H.-J. Jentschel, "Direct conversion receivers - expectations and experiences," in RF Front End Architectures, IEEE MTT-S 2000, Boston, Workshop, June 2000.
- [13] S. O. Haykin, Adaptive Filter Theory. Prentice Hall, 2001.
- [14] H. Meyr, M. Moeneclaey, and S. A. Fechtel, Digital Communication Receivers. Wiley, 1996.